ORIGINAL PAPER

Analysis of tropospheric warming and stratospheric cooling in the present and future climate from the suite of CMIP6 models

T. V. Lakshmi Kumar[1,2] · G. Purna Durga[1] · A. Aravindhavel[2] · Humberto Barbosa[3] · D. Narayana Rao[2,4]

Abstract

Warming in the upper troposphere and cooling in the lower stratosphere are one of the important atmospheric processes since mid of the twentieth century. Present work focuses on analyzing the Newtonian cooling coefficients (NCCs) over different hemispheric regions of lower stratosphere using the temperature data sets of multi-model mean (MMM) obtained from the simulations of fifteen (15) general circulation models' of the Coupled Model Intercomparison Project (CMIP) phase 6. Spatiotemporal trends of temperature showed the highest warming and cooling of 1.28°K and 1.68°K over tropical regions of the northern hemisphere at 250 and 30 hPa levels respectively. The wave kinetic energies of the lower stratosphere showed a decreasing trend which is an indication of continuous cooling over different latitudinal regions. The NCC is found high (varied up to 3.456°K) with reference to the standard atmospheric profile of 1976 over the northern and southern hemisphere (NH) tropical regions and is pronounced in the period 2071 to 2100 under the fifth shared socioeconomic pathway (SSP) of CMIP 6.

1 Introduction

Trends in vertical atmospheric temperature profiles have attained paramount importance in climate change research (Seidel et al. 2011). The two way interactions of troposphere and stratosphere show implications on climate change (Sigmond et al. 2008). Observations and model results report the increased stratospheric CO_2 levels, scattered radiation from volcanic aerosols along with the variations in solar irradiance in stratosphere, influence the tropospheric dynamics by means of affecting the amplitudes of planetary waves and the intensity of Hadley cell (Rind and Lacis 1993). Several researchers reported the warming in the troposphere and cooling in the lower stratosphere using radiosonde and satellite observations (Rao et al. 2007, Titchner et al. 2009, Zou et al. 2009, Haimberger et al. 2012). Steiner et al. (2020)

used the radio occultation (RO) measurements and found warming of 0.25 to 0.35°K per decade during 2002 to 2018 and 1 to 3°K cooling in the lower stratosphere during the last four decades when analyzed with the combined data sets of RO, radiosondes, and lidars. Depletion of the stratospheric ozone and increased greenhouse gas emissions are reported to be the reason for warming in troposphere and cooling of lower stratosphere (Randel et al. 2017). Wang et al. (2020) also reported that the increased CO_2 is responsible for an increase in tropospheric temperatures. Increased CO_2 concentrations at troposphere levels become optically thin to transmit the outgoing infrared radiation which is responsible for radiative cooling in the stratospheric regions (Manabe and Strickler 1964). Stratospheric heating is mainly because of absorption of UV and infrared radiation by ozone and near infrared absorption by CO2 and water vapor. With the increase in CO2 concentration in the stratosphere, emission dominates the absorption leading to infrared cooling at all levels of stratosphere (https://archive.ipcc.ch/ipccreports/tar/wg1/278.htm). The surface temperature rapidly responses to the radiative forcing when the relative humidity is fixed and hence, the distribution of relative humidity has more sensitivity to the radiative forcings causing either cooling or warming (Bourdin et al. 2021).

Though there is a partial recovery of stratospheric ozone from 1998 to 2014 (Randel et al. 2017), the general circulation models continue to show the cooling at lower

✉ T. V. Lakshmi Kumar
   lkumarap@hotmail.com

1   Atmospheric Science Research Laboratory, Department of Physics, SRM Institute of Science and Technology, Chennai, Kattankulathur, India

2   Satellite Meteorology Cell, SRM Institute of Science and Technology, Kattankulathur, India

3   Universidade Federal Alagoes, Meico, Brazil

4   SRM University AP, Andhra Pradesh, India

stratosphere for the past 60 years (Santer et al. 2013) amidst the role of volcanic eruptions. However, Ball et al. (2018) reported that the ozone in the lower stratosphere continues to decline while in the upper stratosphere shows the recovery. As the stratospheric dynamics influence the tropospheric circulation (ex: stratosphere — troposphere exchanges known as Brewer — Dobson circulation (Butchart 2014)), the CMIP 5 models have been evolved by incorporating the complete stratospheric features in the model development (IPCC 2013). Coupled Model Intercomparison Project models have been used for studying the characteristics of the upper troposphere and lower stratosphere by means of analyzing the tropical tropopause layer (Lin et al. 2017), stratospheric ozone (Xia et al. 2018), and cold point tropopause region (Kim et al. 2013). It is reported that the general circulation models show lesser/more warming/cooling of troposphere/stratosphere when compared with the satellite estimates (Santer et al. 2013). A coupled surface–atmosphere climate feedback response analysis method (CFRAM), one of the CMIP5 models, studied stratospheric cooling and found the radiative processes dominate the observed cooling under the Representative Concentration Pathway (RCP) 8.5 future climate scenario (Yang et al. 2016). A study on the performance of the observations, reanalyses, CMIP3, and CMIP5 simulations unraveled the discrepancies on the trends of temperatures over the upper troposphere and lower stratosphere (Xu et al. 2013). Hence, it is interesting to know the trends of temperatures and their warming/cooling over the troposphere/stratosphere using the newly emerged data sets of CMIP6.

The general circulation in the middle atmosphere, i.e., from 15 to 50 kms is mainly driven by the radiative processes, particularly the radiatve heating (Holton 2002). The radiative heating due to the absorption of solar insolation by O_3 and O_2 is largely balanced by the radiative cooling exerted due to the absorption of outgoing thermal infrared by CO_2 and O_3 at troposphere levels. A method called cooling to space approximation is used to estimate the cooling rates in stratosphere and beyond to understand the cooling that has major bearing on temperatures (Liou 2002). This method considers the upward and downward fluxes by neglecting the variation in Plank fluxes. Also, the cooling rates estimated from this approach are mainly from the emisisons of local layers (Liou 2002). The present investigation focuses on reporting the temperature trends of upper troposphere and lower stratosphere and the Newtonian cooling coefficients for the lower stratosphere using the multi-model mean of CMIP6 data sets during the historical and future climate scenario. The main objectives of the work are:

- Spatiotemporal analysis of temperature and its trends over troposphere and stratosphere from multi-model mean (MMM) of CMIP6 GCM outputs for the period 1986 to 2014
- Analysis of wave kinetic energies at lower stratosphere for the period 1986 to 2014 using NCEP reanalysis data
- Analysis of the vertical Newtonian cooling coefficients in the present and future climate scenario of SSP5.

2 Data and methods

We have used the temperature data sets of fifteen (15) CMIP 6 general circulation models' simulations that are listed in Table 1 (https://esgf-node.llnl.gov/search/cmip6), to obtain the multi-model mean (MMM) which has been used to study the objectives of the present study. While preparing the MMM, all the models have been brought to uniform

Table 1 List of CMIP6 models used to obtain the MMM in the present study

S.No	CMIP 6 model	Country	Horizontal Resolution	Key reference
1	ACCESS-CM2	Australia	1.9°×1.3°	Bi et al. (2012)
2	ACCESS-ESM1	Australia	1.9°×1.2°	Law et al. (2017)
3	BCC-CSM2-MR	China	1.1°×1.1°	Wu et al. (2019)
4	CAMS-CSM1-0	China	1.1°×1.1°	Rong et al. (2019)
5	CanESM5	Canada	2.8°×2.8°	Swart et al. (2019)
6	CESM2-WACCM	USA	1.3°×0.9°	Liu et al. (2019)
7	FGOALS-g3	China	2°×2.3°	Reference
8	FIO-ESM-2–0	China	1.3°×0.9°	Song et al. (2019)
9	MIROC6	Japan	1.4°×1.4°	Tatebe et al. (2019)
10	MPI-ESM1-2-H	Germany	0.9°×0.9°	Gutjahr et al. (2019)
11	MPI-ESM1-2-L	Germany	1.9°×1.9°	Mauritsen et al. (2019)
12	MRI-ESM2-0	Japan	1.1°×1.1°	Yukimoto et al. (2019)
13	NESM3	China	1.9°×1.9°	Cao et al. (2018)
14	NorESM2-LM	Norway	2.5°×1.9°	Seland et al. (2020)
15	NorESM2-MM	Norway	2.5°×1.9°	?

grid resolution of $1° \times 1°$ using bilinear interpolation method (e.g., Almazroui et al. 2017; Sharmila et al. 2015). The advantage of using the multi-model mean (MMM) is to minimize the uncertainties arising from the individual GCMs. Also, bringing the MMM into uniform grid resolution allows the conventional computations more precisely.

The historical period of the data set is considered from 1986 to 2014, and the future scenario from 2021 to 2100 (near future: 2021–2050 and far future: 2071–2100) under SSP5 (RCP5.8.5) is used further. SSPs are developed based on the new emissions and socio economic scenarios. They are developed at a global scale that have future world developments and associated quantification by the integrated assessment models (Riahi et al. 2017). There are five (5) narratives of SSPs, known as (i) SSP1 (sustainability — takes the green road), (ii) SSP2 (middle of the road), (iii) SSP3 (regional rivalry — a rocky road), (iv) SSP4 (inequality — a road divided), and (v) SSP5 (fossil fuel development — taking the highway). The combination of SSPs and RCPs provides information on how society and climate evolve in the future (O'Neill et al. 2020).

We have compared the temperature of MMM of CMIP6 (hereafter referred as MMM) with the satellite-based temperature data sets obtained from the COSMIC global positioning systems radio occultation observations (GPSROs) to understand the agreement of MMM with the satellite measurements. The height resolution of GPSRO varies from 200 m to 1 km. GPSRO provides promising data sets of temperature across the globe from the altitude of 5 to 40 km (Kursinski et al. 1997; Rao et al. 2007; Guo et al. 2011). Since MMM data for the historical period is available till 2014; we have used the mean annual temperature data of COSMIC GPSRO for the comparison purpose at 300 and 50 hPa levels during the period 2007 to 2014. Due to the inadequate coverage of radiosondes globally, we could not compare the MMM data sets with the temperature of radiosondes globally. The poor coverage of radiosondes in tropics, southern hemisphere, and the limitations of radiosonde data when considered globally had been very well discussed by Hurrel et al. (2000) and Agudelo and Curry (2004).

Monthly wind speed and direction from the National Centers for Environmental Prediction (NCEP) reanalysis data with $1° \times 1°$ has been used at the lower stratosphere levels.

To estimate the wave kinetic energy (KE), the following formula has been used Eq. 1:

$$KE = 1/2(u^2 + v^2) \tag{1}$$

The wave kinetic energies have been calculated for the lower stratospheric heights for the period 1986 to 2014.

Furthermore, we estimated the Newtonian cooling coefficients over the upper tropospheric and lower stratospheric

heights compared to the standard atmospheric profile of 1976.

Newtonian cooling coefficient ao(z) for small departures from the reference temperature profile To(z), i.e., if Q (T) is the infrared cooling rate for a temperature profile T(z), then:

$$ao(z) = \frac{1}{2}\delta^{-1}\{Q(To + \delta) - Q(To - \delta)\} \tag{2}$$

where δ is a small perturbation (0.1°K). The cooling coefficient ao(z) is obtained for perturbations from the 1976 standard atmosphere profile.

To correct for variation of the cooling coefficient with variations of temperature in order to get a cooling coefficient a (z) valid over a wider range of temperatures, we use Eq. 3:

$$a(z) = ao(z)\{1 + b[T(z) - To(z)]\} \tag{3}$$

where b is a constant, chosen in some sense to minimize the resulting error. On the basis of a simple fit to the second term in a Taylor's series expansion of the Planck function, a tentative choice for b for the pressure greater than 0.2mb is Eq. 4:

$$b = \frac{0.0033}{To(z) - 135} \tag{4}$$

Infrared cooling rate (Q) from the Eq. (2) can be computed from the following expression Eq. 5:

$$Q(z) = \frac{dTr}{dz}(z, Z)[Br(Z) - Br(top)] \tag{5}$$

$$-\frac{dTr}{dz}(z, 0)\big[Br(0) - Br(g)\big]$$

$$-\int_0^z \frac{dTr}{dz}(z, z^1)\frac{dBr}{dz}(z^1)dz^1$$

In the above equation, where Br(z) represents the Planck's function for the air temperature at level z, the ground is "g," the highest level is "Z." is the temperature at a level of consideration.

Planck's function Br(z) has been calculated from the temperature at that level and wavelength of the infra-red radiation at 15 µ is considered.

The procedure mentioned above for calculating NCC is proposed in Dickinson, 1973 and is widely used for the same purpose over different latitudinal regions (Wehrbein and Leovy 1982; Jucker et al. 2014; Calvo et al. 2017).

The NCCs have been computed and analyzed for the historical period 1986 to 2014 as well as for the future climate change scenarios of SSP5 for the epochs 2021 to 2050 and 2071 to 2100.

3 Results and discussion

3.1 Comparison of temperature from COSMIC GPSRO and MMM of CMIP6 and its trends

Comparisons of mean annual temperature obtained from the COSMIC GPSRO and MMM of CMIP6 for the pressure levels 300 and 50 hPa are provided in Fig. 1a–d for the study period 2007 to 2014. Visual inspection of Fig. 1 infers a good agreement in the temperature pattern of both data sets at the two levels. Both the data sets well depicted the warming and cooling over tropical latitudes. The mean annual global mean temperatures for the study period at 300/50 hPa obtained from GPS RO and MMM of CMIP 6 are 229.00/212.00°K and 228.28/210.99°K respectively. We find the distinguished biases between COSMIC GPSRO and MMM when the temperature data is averaged zonally for different hemispheric belts. Higher bias is observed in the southern hemisphere at both 300 hPa and 50 hPa levels. In most of the hemispheric regions, a bias upto 2.5°K is observed in all hemispheric belts with no bias at 300 hPa of northern hemispheric tropics. Overall analysis shows that the MMM of CMIP6 underestimates the atmospheric temperature obtained from the GPS RO at 300 and 50 hPa levels from 2007 to 2014. The bias of ± 2 K has been reported by Kishore et al. (2016) when

GPSRO and ensemble of 17 general circulation models of CMIP5 were compared for the period 2006 to 2013. Also, it is reported that the bias between GPS RO and CMIP5 was found to decrease with the altitude and the same turned to cold bias at higher altitudes (Kishore et al. 2016). It is worth noting that the comparison of GPS RO with radiosonde profiles of temperature over different regions across the globe revealed the COSMIC GPSRO has sufficiently high accuracy in representing the radiosondes (Kuo et al. 2005).

Figure 2 depicts the spatial pattern of linear trend per year for the mean annual temperatures at different pressure levels obtained from the MMM of CMIP6 data sets for the historical period 1986 to 2014. Tropical regions of the northern and southern hemispheres are found that they have undergone a higher degree of warming at the upper-tropospheric levels (300, 200, and 100 hPa) during the study period. This is followed by mid-latitude and polar regions, where the southern polar latitudes have shown the least warming compared to other latitudinal regions. The trend over the tropical regions gradually changed to cooling from warming as the height increases, i.e., when the lower stratosphere is reached. Remarkably, the trend at 30 hPa has shown the highest cooling trend over the tropics and is followed by mid and polar latitudes.

The magnitudes of warming and cooling at different levels when averaged zonally over the hemispheric regions are

Fig. 1 Mean annual temperature observed from **a** and **c** COSMIC GPSRO and **b** and **d** CMIP 6 MMM at **a** and **b** 300 hPa and **c** and **d** 50 hPa for the period 2007 to 2014
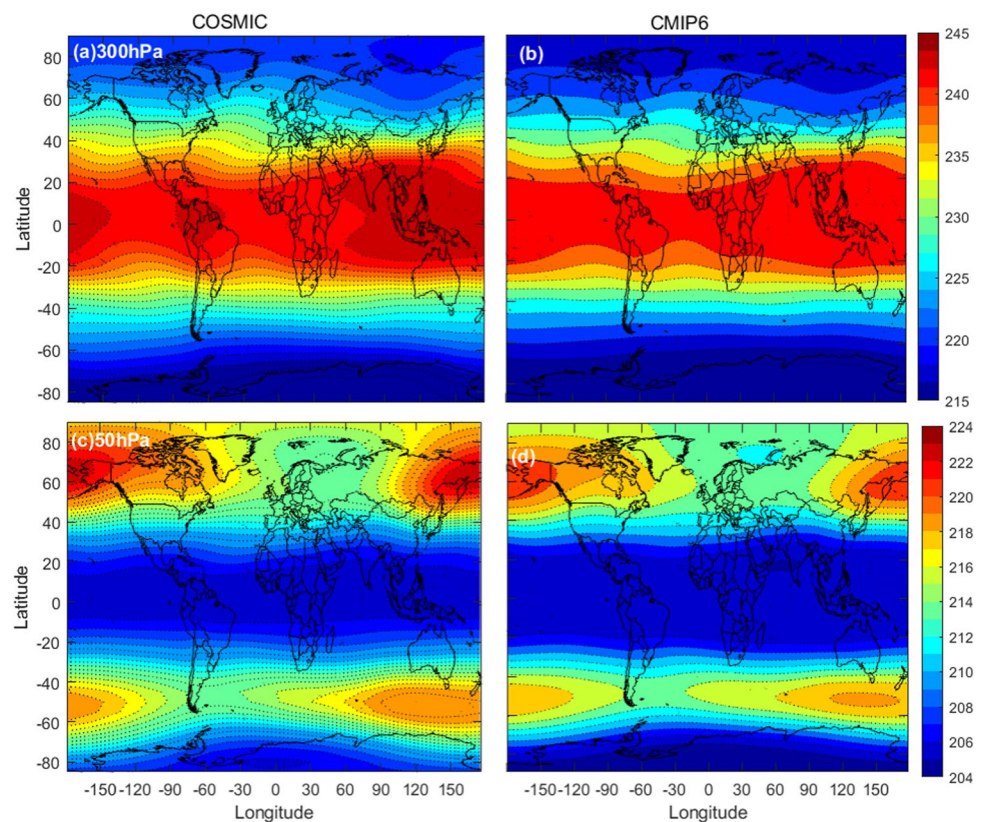
Fig. 2 Trends (per year) of mean annual temperature for the period 1986–2014 at different pressure levels
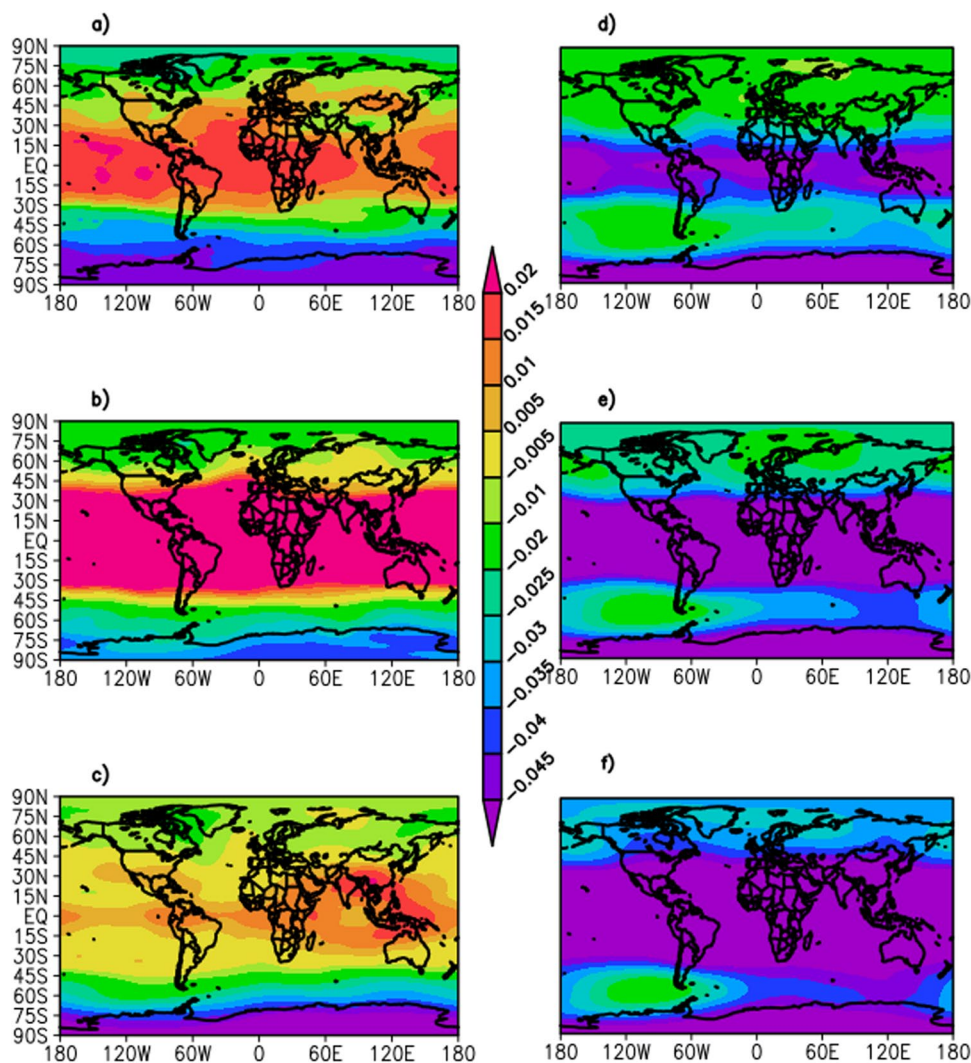

Table 2 Magnitudes of warming and cooling for the period 1986 to 2014 for different hemispheric belts

Pressure	Northern hemisphere			Southern hemisphere		
	Tropics	**Mid latitudes**	**Poles**	**Tropics**	**Mid latitudes**	**Poles**
300 hPa	+1.26	+1.00	+0.74	+1.23	+0.65	+0.26
250 hPa	+1.28	+0.74	+0.28	+1.25	+0.45	−0.11
200 hPa	+1.21	+0.22	−0.37	+1.19	−0.06	−0.86
150 hPa	+1.00	−0.05	−0.28	+0.96	−0.39	−1.12
100 hPa	+0.24	−0.05	−0.23	+0.19	−0.34	−1.13
70 hPa	−1.02	−0.43	−0.38	−1.13	−0.66	−1.24
50 hPa	−1.67	−0.79	−0.58	−1.62	−0.87	−1.28
30 hPa	−1.68	−1.15	−0.86	−1.58	−1.05	−1.17
20 hPa	−1.53	−1.32	−1.06	−1.49	−1.20	−1.06
10 hPa	−1.54	−1.57	−1.32	−1.53	−1.44	−1.19

provided in Table 2. From the Table 2, it can be seen that the transition of warming to cooling over tropical belts in between to 100 hPa (~ 16 km) to 70 hPa (18 km) and the highest cooling has been observed at 29 km (30 hPa) in

these regions. In northern mid latitudes, a highest warming of 1°K is observed at 300 hPa and the least warming in the same region of southern hemisphere which is about 0.19°K at 100 hPa. Tropics of the SH showed the highest cooling

(− 1.66°K) at 30 hPa. From the table, we can observe that the transition of warming in the upper troposphere to cooling in the lower stratosphere through the tropopause in all the hemispheric regions. The warming in the upper troposphere is also reported by Santer et al. (2017) by using the satellite data sets such as Remote Sensing Systems (RSS), Center for Satellite Applications and Research (STAR), and University of Alabama Huntsville (UAH), along with the ensemble of five global climate model simulations of CMIP5. Santer et al. (2017) also reported that the magnitude of warming in the mid to upper troposphere is higher than that of obtained from the model estimates. When studied with the ensemble model simulations of natural and anthropogenic forcings along with the RCP 8.5 simulations, the lower stratosphere has shown the cooling trend for the past 60 years (Santer et al. 2013) which was mainly reported due to the depletion of stratospheric ozone.

The latitudinal variation of temperature at different levels from 1986 to 2014 is shown in Fig. 3. Figure 3 indicates the transition of warming to cooling, particularly over tropical and subtropical latitudes. Deep tropical regions show a temperature above 240°K at 300 hPa and slowly diminished below 195°K at 30 hPa level. A temperature difference of around 45°K is observed in the deep tropical regions between the upper troposphere and lower stratosphere while this difference of temperature between the same is only 15°K over the high latitudes. Similar variations were observed in temperature at 500 hPa (middle troposphere) and 50 hPa (lower stratosphere), wherein the transition changes of warming to cooling were found high in tropical regions (Cordero et al. 2006). The transition of warming to

cooling in mid and polar latitudes is not as much as observed in deep and extratropical regions. It is reported that tropospheric warming is mainly linked to latent heating, while the increased convection is the reason for radiative cooling, resulting in lower stratospheric cooling (Zhang et al. 2016). Strong latitudinal variations in stratospheric ozone play a critical role in temperature transitions in the upper troposphere and lower stratosphere (Seidel et al. 2011).

3.2 Wave kinetic energies from the NCEP reanalysis data sets and Newtonian cooling coefficients for historical and future SSP5 scenario of CMIP 6

Our main objectives are also on the estimation of Newtonian cooling coefficients (NCCs) in comparison with the standard atmospheric profile, for the historical period 1986 to 2014 along with the future epochs (2021 to 2050 and 2071 to 2100) under the SSP5 climate change scenario. Before this analysis, we have carried out the analysis on the wave kinetic energies to understand stratospheric cooling. Wave perturbations are very important in deciding the energy of waves. More fluctuations result in more kinetic energy, and low perturbations yield less energy. As the kinetic energy is proportional to the square root of temperature, the wave kinetic energy can be used as a proxy to understand the temperature variations within the region.

In Fig. 4, we estimate the trends of wave kinetic energy (normalized with mean) for the period 1986 to 2014 during the January month over the northern hemisphere and July month over the southern hemisphere, i.e., concentrated on winter months. We have estimated these trends for the lower

Fig. 3 Latitudinal variation of atmospheric temperature for different heights obtained from MMM of CMIP6 for the period 1986 to 2014
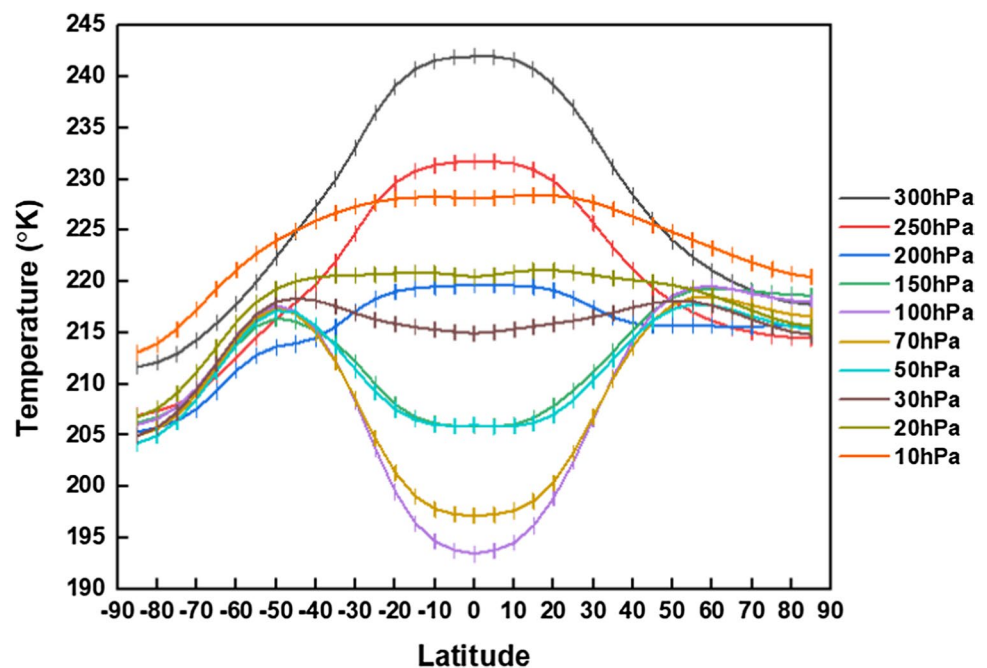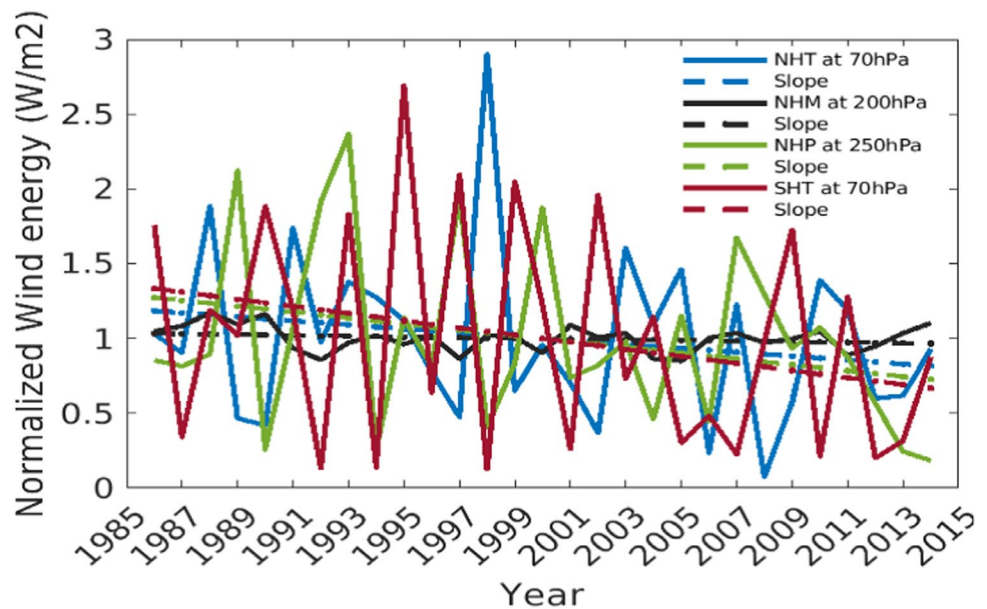
Fig. 4 Trends in kinetic energy of the waves at lower stratospheric level obtained from NCEP data of 1986 to 2014 during winter (January) of northern and southern hemisphere

stratospheric regions, i.e., just above the tropopause. The tropopause height for tropics is approximately at 100 hPa (16 km), mid-latitudes is 250 hPa (11 km), and for poles is 300 hPa (8 km). Hence, we tried just above these levels to show that the wave kinetic energy is declining at lower stratospheric levels. The trends obtained in this analysis are statistically significant at 0.01 and 0.05 levels. We found the trends of wave kinetic energy is significantly decreasing during the study period 1986 to 2014 over NH and SH tropics. Also, we found significant decreasing trends over just above the tropopause of NH mid and polar latitudes. However, the decreasing trends over middle and polar latitudes of the southern hemisphere are not as much as in northern hemispheric middle and polar latitudes. A study of Rind et al. (2005) reported that the changes in eddy energy affect the angular momentum transport due to its poleward transport of angular momentum over the mid-latitudes and the equatorward transport over the high latitudes and found the kinetic energy conversion is decreasing in the global warming experiments. In the present analysis, we have also seen the same feature of decreasing kinetic energy, which indicates global warming that is resulted in stratospheric cooling.

Figure 5 shows the NCCs calculated with reference to the standard atmospheric profile of 1976 for the historical period 1986 to 2014 and for the scenario of fossil fuel development (SSP5 for the epochs 2051 to 2070 and 2071 to 2100. Vertical profiles of NCCs show a perceptible change in cooling for the study epochs. The cooling is less at upper tropospheric levels of all the regions and gradually altered and showed the mixing pattern as it goes high during the period 1986 to 2014, when compared to the oter epochs. The tropical regions of NH and SH show the higher side of cooling from the

upper-tropospheric level and continued till the lower stratospheric levels, i.e., up to 70 hPa. After that, the NCC started decreasing in the future epochs. The same feature is observed in the mid latitudinal and polar regions. The magnitude of NCC is high for the future periods compared to the historical period till the lower stratospheric levels, i.e., till 150 hPa and 250 hPa, respectively. The NCCs are submerged over the polar latitudes above the lower stratospheric levels. In all the regions, the NCCs of the epoch 2071 to 2100 showed higher values compared to the periods 1986 to 2014 and 2021 to 2050 at lower stratospheric altitudes. The magnitudes of NCC varied from 3.4 to 3.5°K during all the periods. Another interesting feature observed from Fig. 5 is that the NCC has shown distinct differences beyond the lower stratospheric regions in the respective hemispheric belts. It is to be noted that the estimation of NCC considers the radiative relaxation temperature and damping gradients that are independent of latitude as described in Ming et al. (2016). The latitudinal variations of NCC exist in the present analysis due to the externally imposed dynamic considerations. The distinct NCCs above 70 hPa may also be attributed to latitudinal gradients in ozone, temperature profiles, and water vapor (Ming et al. 2016). The overall analysis of NCCs shows that the general circulation models of CMIP6 can show lower stratospheric cooling in response to the global warming experiments in the historical and complete fossil fuel development scenarios.

4 Conclusions

As it is well documented that the stratospheric dynamics influence the tropospheric circulation and thus the surface climate, understanding the stratospheric processes helps
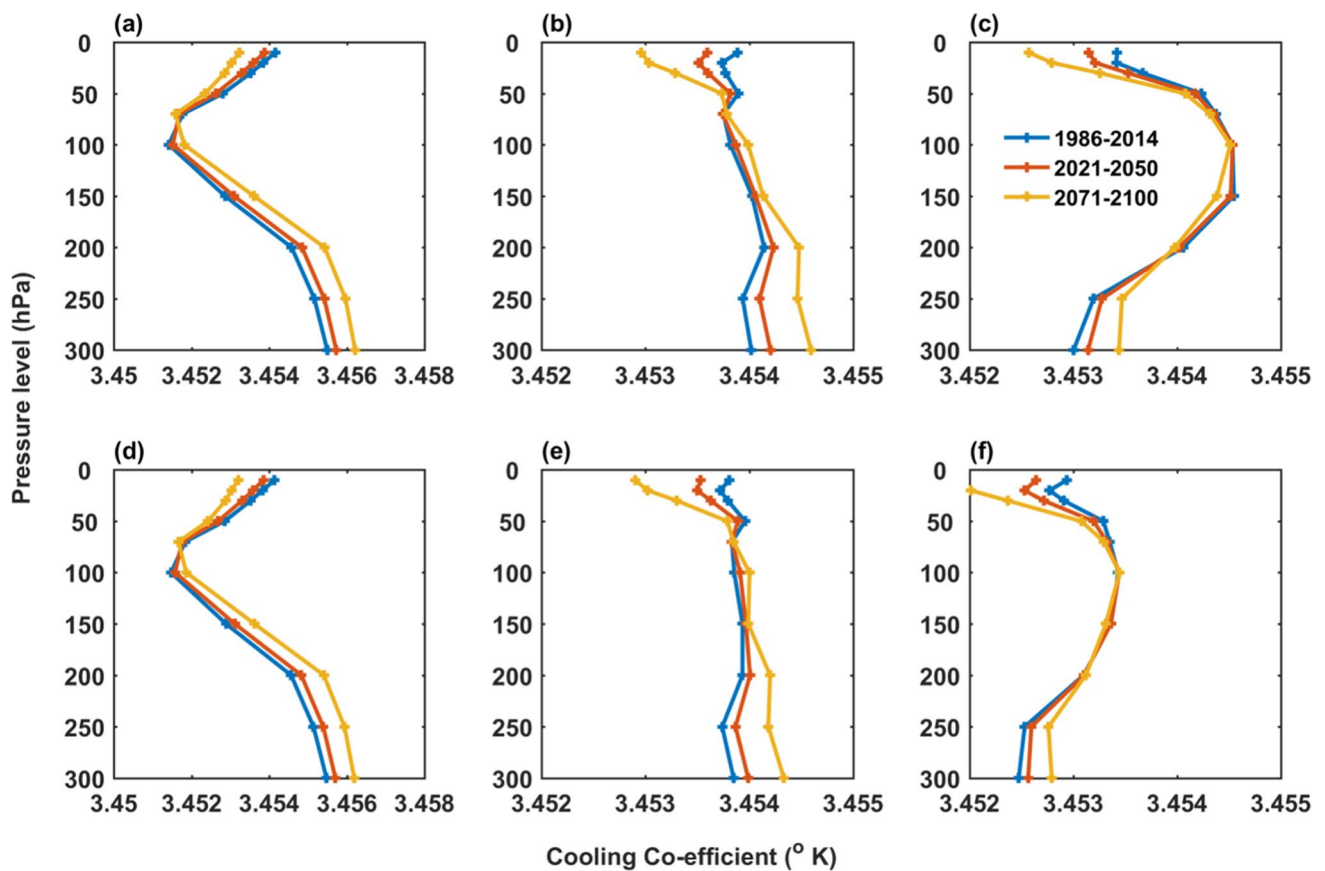
Fig. 5 Newtonian cooling coefficients obtained from the CMIP6 data sets for the SSP 5 future scenario with reference to the standard atmospheric profile of 1976.(NHT — northern hemisphere: tropics; NHM — northern hemisphere mid latitudes; NHP — northern hemisphere poles; SHT — southern hemisphere tropics; SHM — southern hemisphere mid latitudes; and SHP — southern hemisphere poles)

the scientific community for better modeling of troposphere. Sudden stratospheric warmings are found to have connection with the surface climate. Also, the precursors of atmospheric blocks found in stratosphere which causes extreme weather in mid and high latitudes. The cooling in the stratosphere is also reported to have linkage with the diabatic heating from the troposphere. These atmospheric processes will be enhanced in the future climate change scenarios. The studies on stratospheric cooling in the present and future climate change play a vital role in understanding the surface climate mechanisms. Hence, the present study focuses on understanding the lower stratospheric cooling and upper tropospheric cooling using the newly emerged CMIP 6 GCMs' simulations. The conclusions from the results of the study are:

MMMs of CMIP6 showed the trends of warming and cooling over the upper troposphere and lower stratosphere and are more prominent in tropical regions.
The transition of warming to cooling from the upper troposphere to the lower stratosphere is characterized by the more differences in temperature over tropics than the mid-latitudes and poles.

The NCCs are found to varied up to 3.456°K with respect to the standard atmospheric profile of 1976. More cooling in the lower stratosphere has been observed in the epoch 2071 to 2100 under the SSP5 future climate change scenario compared to previous periods.

Declarations

Ethics approval Not applicable.

Consent to participate Not applicable.

Consent for publication The authors have no objection for the publication.

Conflict of interest The authors declare no competing interests.

References

Agudelo PA, Curry JA (2004) Analysis of spatial distribution in tropospheric temperature trends. Geophys Res Lett 31:L22207. https://doi.org/10.1029/2004GL020818

Almazroui M, Nazrul Islam M, Saeed S, Alkhalaf AK, Dambul R (2017) Assessment of uncertainties in projected temperature and precipitation over the Arabian Peninsula using three categories of Cmip5 multimodel ensembles. Earth Syst Environ 1(2):1–20

Ball WT et al (2018) Evidence for a continuous decline in lower stratospheric ozone offsetting ozone layer recovery, Atmos. Chem Phys 18:1379–1394

Bi D, Dix M, Marsland S, O'Farrell S, Rashid H, Uotila P, Hirst KE, Golebiewski SA, Yan Y, Franklin C, Hannah SZ, Vohralik W, Fiedler R, Collier M, Puri K (2012) The ACCESS coupled model: description, control climate and evaluation. Aust Meteorol Oceanogr J 63:41–4. https://doi.org/10.22499/2.6301.004

Butchart N (2014) The brewer-dobson circulation, reviews of geophysics. https://doi.org/10.1002/2013RG000448

Cao J, Wang B, Yang Y-M, Ma L, Li J, Sun B, Bao Y, He J, Zhou X, Wu L (2018) The NUIST Earth System Model (NESM) version 3: description and preliminary evaluation. Geosci Model Dev 11:2975–2993

Cordero EC, de Forster PM, F, (2006) Stratospheric variability and trends in models used for the IPCC AR4. Atmos Chem Phys 6:5369–5380

Dickinson RE (1973) Method of parameterization for infrared cooling between altitudes 30 and 70 kilometers. J Geophys Res 78(21):4451–4457

Gutjahr O, Putrasahan D, Lohmann K, Jungclaus JH, von Storch J-S, Brüggemann N, Haak H, Stössel A (2019) Max Planck Institute Earth System Model (MPI-ESM1.2) for the High-Resolution Model Intercomparison Project (HighResMIP). Geosci Model Dev 12:3241–3281

Haimberger L, Tavolato C, Sperka S (2012) Homogenization of the global radiosonde temperature dataset through combined comparison with reanalysis background series and neighboring stations. J Climate 25:8108–8131. https://doi.org/10.1175/JCLI-D-11-00668.1

Holton JR (2002) Encyclopedia of Atmospheric Sciences. Academic Press, USA

Hurrel JW et al (2000) Comparison of tropospheric temperatures from radiosondes and satellites: 1979–98. Bull Am Meteorol Soc 81:2165–2177

IPCC (2013) Climate change 2013: the physical science basis. Working group I contribution to the fifth assessment report of the intergovernmental panel on climate change. In: Stocker TF, Qin D, Plattner G-K, Tignor M, Allen SK, Boschung J, Nauels A, Xia Y, Bex V, Midgley PM (eds) Cambridge University Press, Cambridge, pp 1535

Kursinski E, Hajj GA, Schofield JT, Linfield RP, Hardy KR (1997) Observing earth's atmosphere with radio occultation measurements using the global positioning system. J Geophys Res Atmos 102:D23429–D23465

Law RM, Ziehn T, Matear RJ, Lenton A, Chamberlain MA, Stevens LE, Wang Y-P, Srbinovsky J, Bi D, Yan H, Vohralik PF (2017) The carbon cycle in the Australian Community Climate and Earth System Simulator (ACCESS-ESM1)—Part 1: model description and pre-industrial simulation. Geosci Model Dev 10:2567–2590. https://doi.org/10.5194/gmd-10-2567-2017

Liou KN (2002) An introduction to atmospheric radiation. Academic Press, USA, International Geophysics Series

Liu S-M, Chen Y-H, Rao J, Cao C, Li S-Y, Ma M-H, Wang Y-B (2019) Parallel comparison of major sudden stratospheric warming events in CESM1-WACCM and CESM2-WACCM. Atmosphere 10:679

Manabe S, Strickler F (1964) Thermal equilibrium of the atmosphere with a convective adjustment. J Atmos Sci 21:361–385

Mauritsen T, Bader J, Becker T, Behrens J, Bittner M, Brokopf R et al (2019) Developments in the MPI-M Earth System Model version 1.2 (MPI-ESM1.2) and its response to increasing CO2. J Adv Model Earth Syst 11:998–1038

O'Neill BC, Carter TR, Ebi K et al (2020) Achievements and needs for the climate change scenario framework. Nat Clim Chang 10:1074–1084. https://doi.org/10.1038/s41558-020-00952-0

Riahi K, van Vuuren DP, Kriegler E, Edmonds J, O'Neill BC et al (2017) The shared socioeconomic pathways and their energy, land use, and greenhouse gas emissions implications: an overview. Glob Environ Chang 42:153–168

Rind D, Lacis A (1993) The role of the stratosphere in climate change. Surv Geophys 14:133–165. https://doi.org/10.1007/BF02179221

Rong XY, Li J, Chen HM et al (2019) Introduction of CAMS-CSM model and its participation in CMIP6. Clim Change Res 15(5):540–544. https://doi.org/10.12006/j.issn.1673-1719.2019.186

Seidel DJ, Gillet NP, Lanzante JR, Shine KP, Thorne PW (2011) Stratospheric temperature trends: our evolving understanding, WIRES Clim. Chang 2:592–616

Song ZY, Ying BAO, Fang-Li QIAO (2019) Introduction of FIO-ESM v2.0 and its participation plan in CMIP6 experiments. Clim Change Res 15(5):558–565

Swart NC, Cole JNS, Kharin VV, Lazare M, Scinocca JF, Gillett NP, Anstey J, Arora V, Christian JR, Hanna S, Jiao Y, Lee WG, Majaess F, Saenko OA, Seiler C, Seinen C, Shao A, Sigmond M, Solheim L, von Salzen K, Yang D, Winter B (2019) The Canadian Earth System Model version 5 (CanESM5.0.3). Geosci Model Dev 12:4823–4873

Tatebe H, Ogura T, Nitta T, Komuro Y, Ogochi K, Takemura T, Sudo K, Sekiguchi M, Abe M, Saito F, Chikira M, Watanabe S, Mori M, Hirota N, Kawatani Y, Mochizuki T, Yoshimura K, Takata K, O'ishi R, Yamazaki D, Suzuki T, Kurogi M, Kataoka T, Watanabe M, Kimoto M (2019) Description and basic evaluation of simulated mean state, internal variability, and climate sensitivity in MIROC6. Geosci Model Dev 12:2727–2765

Titchner HA, Thorne PW, McCarthy MP, Tett SFB, Haimberger L, Parker DE (2009) Critically reassessing tropospheric temperature trends from radiosondes using realistic validation experiments. J Climate 22:465–485. https://doi.org/10.1175/2008JCLI2419.1

Wehrbein WM, Leovy CB (1982) An accurate radiative heating and cooling algorithm for use in a dynamical model of the middle atmosphere. J Atmos Sci 39:1532–1544

Wu T, Lu Y, Fang Y, Xin X, Li L, Li W, Jie W, Zhang J, Liu Y, Zhang L, Zhang F, Zhang Y, Wu F, Li J, Chu M, Wang Z, Shi X, Liu X, Wei M, Huang A, Zhang Y, Liu X (2019) The Beijing Climate Center Climate System Model (BCC-CSM): the main progress

from CMIP5 to CMIP6. Geosci Model Dev 12:1573–1600. https://doi.org/10.5194/gmd-12-1573-2019

Xu J, Powell Jr AM, Zhao L (2013) Intercomparison of temperature trends in IPCC CMIP5 simulations with observations, reanalyses and CMIP3 models. Geosci Model Dev 6:1705–1714

Bourdin S, Kluft L and Stevens B (2021) Dependence of climate sensitivity on the given distribution of relative humidity Geophys. Res Lett https://doi.org/10.1029/2021GL092462

Calvo N, Garcia RR and Kinnison DE (2017) Revisiting southern hemisphere polar stratospheric temperature trends in WACCM: the role of dynamical forcing Geophys.Res Lett https://doi.org/10.1002/2017GL072792

Guo P, Kuo YH, Sokolovskiy SV and Lenschow DH (2011) Estimating atmospheric boundary layer depth using COSMIC Radio occultation data JAtmos Sci https://doi.org/10.1175/2011JAS3612.1

Jucker M, Fueglistaler S and Vallis S (2014) Stratospheric sudden warmings in an idealized GCM J Geophys Res Atmospheres https://doi.org/10.1002/2014JD022170

Kim J, Grise KM and Son SW (2013) Thermal characteristics of the cold point tropopause region in CMIP5 models J Geophys Res Atmospheres https://doi.org/10.1002/jgrd.50649

Kishore P, Basha G, VenkatRatnam M, Velicogna I, Ouarda TBMJ and Narayana Rao D (2016) Evaluating CMIP5 models using GPS radio occultation COSMIC temperature in UTLS region during 2006–2013: twenty-first century projection and trends Clim Dyn https://doi.org/10.1007/s00382-016-3024-8

Kuo YH, Schreiner WS, Wang J, Rossiter DL and Zhang Y (2005) Comparison of GPS RO occulation soundings with radiosondes Geophys Res Lett https://doi.org/10.1029/2004GL021443

Lin P, Paynter D, Ming Y and Ramaswamy V (2017) Changes in tropical tropopause layer under global warming https://doi.org/10.1175/JCLI-D-16-0457.1

Ming A, Hitchcock P and Haynes P (2016) The response of lower stratosphere to zonally symmetric thermal and mechanical forcing J Atmos Sci https://doi.org/10.1175/JAS-D-15-0294.1

Randel, WJ, Polvani L, Wu F, Kinnison DE, Zou CZ and Mears C (2017) Troposphere – stratosphere temperature trends derived from satellite data compared with ensemble simulations from WACCM J Geophys Res – Atmospheres https://doi.org/10.1002/2017JD027158

Rao DN Venkat Ratnam M Krishna Murthy BV Jagannadha Rao VVM Mehta SK Nath D and Basha G (2007) Identification of tropopause using bending angle profile from GPS radio occultation (RO): A radio tropopause Geophys Res Lett https://doi.org/10.1029/2007GL029709

Santer BD, Painter JF, Bonfils C, Mears CA, Solomon S, Wigley TM, Gleckler PJ, Schmidt GA, Doutriaux C, Gillett NP, Taylor KE, Thorne PW, Wentz FJ (2013) Human and natural influences on the changing thermal structure of the atmosphere. Proc Natl Acad Sci U S A 110(43):17235–17240. https://doi.org/10.1073/pnas.1305332110

Santer BD, Solomon S, Wentz FJ et al (2017) Tropospheric warming over the past two decades. Sci Rep 7:2336. https://doi.org/10.1038/s41598-017-02520-7

Seland Ø Bentsen M Seland Graff L Olivié D Toniazzo T Gjermundsen A Debernard JB Gupta AK He Y Kirkevåg A Schwinger J Tjiputra J Schancke Aas K Bethke I Fan Y Griesfeller J Grini A Guo C Ilicak M Hafsahl Karset IH Landgren O Liakka J Onsum Moseid K Nummelin A Spensberger C Tang H Zhang Z Heinze C Iverson T Schulz M (2020) The Norwegian Earth System Model, NorESM2—evaluation of theCMIP6 DECK and historical simulations. Geosci Model Dev Discuss 10.5194/gmd-2019-378

Sharmila S Joseph S Sahai AK Abhilash S Chattopadhyay R (2015) Future projection of Indian summer monsoon variability under climate change scenario: an assessment from CMIP5 climate models Glob Planet Change https://doi.org/10.1016/j.gloplacha.2014.11.004

Sigmond M Scinocca JF and Kushner PJ (2008) Impact of the stratosphere on tropospheric climate change Geophys Res Lett https://doi.org/10.1029/2008GL033573

Steiner AK et al (2020) Observed temperature changes in the troposphere and stratosphere from 1979 to 2018 J Clim https://doi.org/10.1175/JCLI-D-19-0998

Wang T Zhang Q Kuilman M and Hannachi A (2020) Response of stratospheric water vapor to CO2 doubling in WACCM ClimDyn https://doi.org/10.1007/s00382-020-05260-z

Xia Y, Huang Y and Hu Y (2018) On the climate impacts of upper tropospheric and lower stratospheric ozone J Geophys Res - Atmospheres https://doi.org/10.1002/2017JD027398

Yang Y, Ren RC and Cai M (2016) Towards a physical understanding of stratospheric cooling under global warming through a process based decomposition method ClimDyn https://doi.org/10.1007/s00382-016-3040-8

Yukimoto S Kawai H Koshiro T Oshima N Yoshida K Urakawa S Tsujino H Deushi M Tanaka T Hosaka M Yabu S Yoshimura H Shindo E Mizuta R Obata A Adachi Y Ishii M (2019) The Meteorological Research Institute Earth System Model version 2.0, MRI-ESM2.0: description and basic evaluation of the physical component. J Meteorol Soc Jpn

Zhang K, Randel WJ and Fu R (2016) Relationship between outgoing longwave radiation and diabatic heating in reanalsesClim Dyn https://doi.org/10.1007/s00382-016-3501-0

Zou CZ, M Gao and M D Goldberg (2009) Error structure and atmospheric temperature trends in observations from the microwave sounding unit. J Climate 22 1661 1681 https://doi.org/10.1175/2008JCLI2233.1